ZAMM · Z. Angew. Math. Mech. **85**, No. 2, 132 – 140 (2005) / **DOI** 10.1002/zamm.200310166

Index analysis and numerical solution of a large scale nonlinear PDAE system describing the dynamical behaviour of Molten Carbonate Fuel Cells

Kurt Chudej[1,*], **Peter Heidebrecht**[2], **Verena Petzet**[1], **Sabine Scherdel**[1,**], **Klaus Schittkowski**[3], **Hans Josef Pesch**[1], **and Kai Sundmacher**[2,4]

[1] Universität Bayreuth, Lehrstuhl für Ingenieurmathematik
[2] Universität Magdeburg, Lehrstuhl für Systemverfahrenstechnik
[3] Universität Bayreuth, Fachgruppe Informatik
[4] Max-Planck-Institut für Dynamik komplexer technischer Systeme, Magdeburg

Received 18 December 2003, revised, and accepted 25 March 2004
Published online 4 February 2005

Key words nonlinear partial differential algebraic equations, time index, spatial index, MOL index, numerical simulation, fuel cells

MSC (2000) 35L80, 65N40, 65L80

This paper deals with the efficient simulation of the dynamical behaviour of Molten Carbonate Fuel Cells (MCFCs). MCFCs allow an efficient and environmentally friendly energy production via electrochemical reactions. Their dynamics can be described by large scale systems of up to currently 22 nonlinear partial differential algebraic equations (PDAE). The paper also serves as a basis for later parameter identification and optimal control purposes. Therefore, the numerical simulations are particularly based on hierarchically embedded systems of PDAE, first of all in one space dimension. The PDAE are of mixed parabolic-hyperbolic type and are completed by nonlinear initial and boundary conditions of mixed type. For a series of embedded models in one space dimension, the vertical method of lines (MOL) is used throughout this paper. For the semi-discretization in space appropriate difference schemes are applied depending on the type of equations. The resulting system of ordinary differential algebraic equations (DAE) in time is then solved by a standard RADAU5 method. In order to justify the numerical procedure, a detailed index analysis of the PDAE systems with respect to time index, spatial index and MOL index is carried through. Because of the nonlinearity of the PDAE system, the existing theory has to be generalized. Moreover, MOL is especially suited for near optimal real time control on the basis of a sensitivity analysis of the semi-discretized DAE system, since a theoretically safeguarded sensitivity analysis does not exist so far for PDAE constrained optimal control problems of the above type. Numerical results complete the paper and show their correspondence with the expected dynamical behaviour of MCFCs.

1 Introduction

Molten Carbonate Fuel Cells (MCFCs) produce electric energy with high efficiency in an environmentally friendly process. Avoiding direct combustion, MCFCs convert chemical energy contained in fuel and oxidizer to electric energy via electrochemical reactions. Although natural gas usually is recommended, MCFCs can be operated by a wide variety of fuels containing non oxidised carbon or hydrogen, as can be found in many industrial processes. Performance, availability and service life of MCFC stacks are greatly dependent on their operating cell temperature which usually lies at about 600 °C.

Due to their relatively high operating temperature, MCFCs are especially promising among the various types of fuel cells, since they do not rely on external reforming, i. e. an external production of hydrogen. External reforming not only increases build-up costs, but also negatively affects the overall energy balance. Moreover, high cell temperatures allow the production of highly valuable heat, which make MCFCs attractive for many industrial applications and for dispersed power supply. On the other hand, the operating temperatures are still low enough to avoid material corrosion, if the cell stacks are controlled properly. Therefore the control of the operation temperature within a specified range and the reduction of temperature fluctuations and gradients are highly desirable to extend the cell's lifespan. These requirements provide the objectives for control purposes, which will be the subject of subsequent papers.

* Corresponding author, e-mail: kurt.chudej@uni-bayreuth.de
** Currently: Universität Bayreuth, Physikalische Chemie II

Principles of operation and first experiences for MCFCs can be found in [4, 8], and [13].

Concerning mathematical modelling of MCFCs, transient models from [2] are used in this paper. They are based on physical phenomena and describe the concentrations of the various chemical species and the associated molar flows in the anode and cathode channels, the temperatures in the gas and solid phases as well as the potential field in the electrode/electrolyte compound. One of the most important features is that these models contain only few restrictions on the current density distribution. For the electrode kinetics a pore model similiar to [12] is applied, which combines Tafel microkinetics with mass transport kinetics. The whole model is presented in dimensionless numbers describing characteristic properties of the system and is taken from [3]. The resulting mathematical model currently consists of up to 22 nonlinear partial differential algebraic equations of mixed parabolic-hyperbolic type together with appropriate initial and boundary conditions.

For more information on the modelling and simulation of various types of fuel cells it is referred to [2].

2 One dimensional models

The physical model is based on the following chemical reactions. Within the gas of the anode channel (flowing from left to right, c. f. Fig. 1) the reforming reaction

$$\mathrm{CH_4} + 2\,\mathrm{H_2O} \rightleftharpoons \mathrm{CO_2} + 4\,\mathrm{H_2}$$

takes place. At the anode and cathode electrode we have the following electro-chemical reactions

$$\mathrm{H_2} + \mathrm{CO_3^{2-}} \rightarrow \mathrm{H_2O} + \mathrm{CO_2} + 2e^-\,,$$

$$\tfrac{1}{2}\mathrm{O_2} + \mathrm{CO_2} + 2e^- \rightarrow \mathrm{CO_3^{2-}}\,.$$

The anode exhaust gas is burned in a combustion chamber and fed into the cathode channel. Carbonate ions are transferred between the electrodes through the electrolyte. The bipolar plate serves as heat conducting material only. From the cell's outside, the electric current can be collected at the electrodes.

This 1D single counter-flow cell model serves as basic physical model of the *Hot Module* concept of the German MTU CFC Solutions GmbH, Munich. Their Hot Module MCFC is made of a stack of 342 cross-flow fuel cells and is now about to become commercially used. It can produce up to 250 kW of electric power at over 50 % overall electric efficiency, not taking into account the exhaust heat. One of the first Hot Modules is operated since October 2002 by the IPF-Heizkraftwerksbetriebsgesellschaft mbH at the electric power station of the Magdeburg University Hospital. Both companies are partners in the aforementioned BMBF sponsored project.

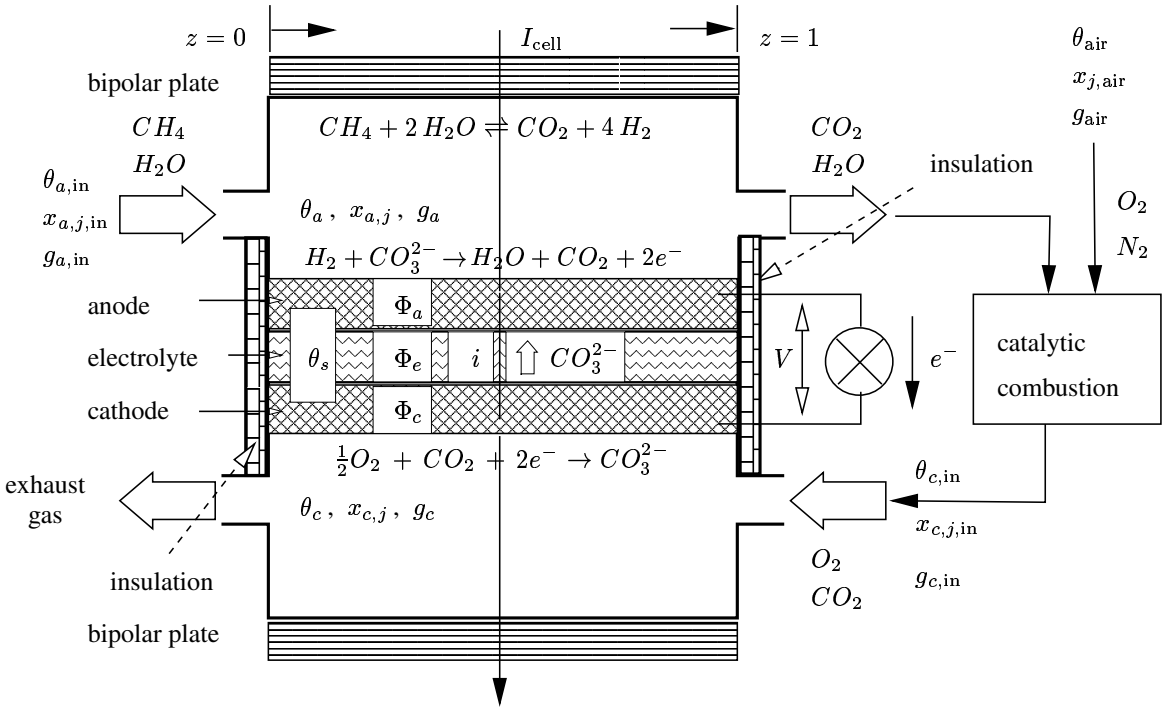

Fig. 1 Working principle of MCFC with internal reforming. Domains, variables, flows, and boundary conditions.

In the following the structure of the underlying mathematical PDAE models is described. All dependent variables of the PDAE systems considered in this paper depend on the spatial variable $z \in [0,1]$ and the time $\tau \in [0,\tau_f]$. The dependent variables are the temperatures of the anode and cathode gas, $\theta_a(\tau,z)$ and $\theta_c(\tau,z)$, resp., the temperature $\theta_s(\tau,z)$ within the solid, i. e. the electrode/electrolyte compound, the molar fractions $x_{a,1}(\tau,z),\ldots,x_{a,n}(\tau,z)$, resp. $x_{c,1}(\tau,z),\ldots,x_{c,n}(\tau,z)$ of the n chemical species ($n=6$, see Table 1) involved in the aforementioned reactions and finally the molar flows $g_a(\tau,z)$ and $g_c(\tau,z)$ in the anode and cathode channels, respectively.

Table 1 Chemical species and their notation.

j	1	2	3	4	5	6
	CH_4	H_2O	H_2	CO_2	O_2	N_2

A more detailed second model also includes the dynamical behaviour of the potential differences $\Phi_a(\tau,z)$, $\Phi_e(\tau,z)$, $\Phi_c(\tau,z)$, and the cell voltage $V(\tau)$ in the electrode/electrolyte compound as well as the current density $i(\tau,z)$; see again Fig. 1.

The first PDAE system of dimension 17 modelling the material and energy balances reads as follows; see [3]:

$$\frac{\partial\theta_s}{\partial\tau} = \lambda\,\frac{\partial^2\theta_s}{\partial z^2} + \varphi_1(\theta_s,\theta_a,\theta_c,x_a,x_c,\Phi_a,\Phi_e,\Phi_c)\,, \tag{1a}$$

$$\frac{\partial\theta_a}{\partial\tau} = -g_a\,\theta_a\,\frac{\partial\theta_a}{\partial z} + \varphi_2(\theta_s,\theta_a,x_a,\Phi_a)\,, \tag{1b}$$

$$\frac{\partial x_{a,j}}{\partial\tau} = -g_a\,\theta_a\,\frac{\partial x_{a,j}}{\partial z} + \varphi_{3,j}(\theta_s,\theta_a,x_a,\Phi_a)\,,\quad j=1,\ldots,n\,, \tag{1c}$$

$$0 = \frac{\partial\,(g_a\,\theta_a)}{\partial z} + \varphi_4(\theta_s,\theta_a,x_a,\Phi_a)\,, \tag{1d}$$

$$\frac{\partial\theta_c}{\partial\tau} = g_c\,\theta_c\,\frac{\partial\theta_c}{\partial z} + \varphi_5(\theta_s,\theta_c,x_c,\Phi_c)\,, \tag{1e}$$

$$\frac{\partial x_{c,j}}{\partial\tau} = g_c\,\theta_c\,\frac{\partial x_{c,j}}{\partial z} + \varphi_{6,j}(\theta_s,\theta_c,x_c,\Phi_c)\,,\quad j=1,\ldots,n\,, \tag{1f}$$

$$0 = \frac{\partial\,(g_c\,\theta_c)}{\partial z} + \varphi_7(\theta_s,\theta_c,x_c,\Phi_c)\,. \tag{1g}$$

If the potential differences Φ_a, Φ_e, and Φ_c are assumed to be constant, we obtain the first simplest 1D model (1). This model can then be hierarchically embedded into a more detailed second 1D model consisting of (1a)–(1g) together with the dynamics (2a)–(2e) for the potential differences Φ_a, Φ_e, and Φ_c and the cell voltage V:

$$\frac{\partial\Phi_a}{\partial\tau} = \big(i - i_a(\theta_s,x_a,\Phi_a)\big)/c_a\,, \tag{2a}$$

$$\frac{\partial\Phi_e}{\partial\tau} = -\big(i - i_e(\Phi_e)\big)/c_e\,, \tag{2b}$$

$$\frac{\partial\Phi_c}{\partial\tau} = -\big(i - i_c(\theta_s,x_c,\Phi_c)\big)/c_c\,, \tag{2c}$$

$$\frac{\mathrm{d}V}{\mathrm{d}\tau} = \Big(\int_0^1 i(\tau,\bar z)\,\mathrm{d}\bar z - I_{\mathrm{cell}}(\tau)\Big)/c_v\,, \tag{2d}$$

completed by the algebraic equation

$$-\Phi_a(\tau,z) + \Phi_e(\tau,z) + \Phi_c(\tau,z) - V(\tau) = 0\,. \tag{2e}$$

The combined model (1), (2) additionally takes into account the charge balances. The complicated nonlinear source terms $\varphi_\diamond$ and $i_\diamond$ ($\diamond$: all indices that apply) can be found in [3]. The quantities $c_\diamond$ and λ are positive constants. The time dependent function $I_{\mathrm{cell}}(\tau)$ denotes the total cell current and can be considered as an input variable of the system which is either to be prescribed or subject to optimization.

The PDAE system (1) is now completed by the following boundary conditions

$$\frac{\partial\theta_s}{\partial z}\Big|_{z=0} = 0\,, \tag{3a}$$

$$\left.\frac{\partial \theta_s}{\partial z}\right|_{z=1} = 0\,, \tag{3b}$$

$$\theta_a(\tau,0) = \theta_{a,\mathrm{in}}(\tau)\,, \tag{3c}$$

$$x_{a,j}(\tau,0) = x_{a,j,\mathrm{in}}(\tau)\,, \quad j=1,\ldots,n\,, \tag{3d}$$

$$g_a(\tau,0) = g_{a,\mathrm{in}}(\tau)\,, \tag{3e}$$

$$\theta_c(\tau,1) = \theta_{c,\mathrm{in}}(g_a(\tau,1), x_a(\tau,1), \theta_a(\tau,1), g_a(\tau,0), x_a(\tau,0))\,, \tag{3f}$$

$$x_{c,j}(\tau,1) = x_{c,j,\mathrm{in}}(g_a(\tau,1), x_a(\tau,1), g_a(\tau,0), x_a(\tau,0))\,, \quad j=1,\ldots,n\,, \tag{3g}$$

$$g_c(\tau,1) = g_{c,\mathrm{in}}(g_a(\tau,1), x_a(\tau,1), g_a(\tau,0), x_a(\tau,0))\,, \tag{3h}$$

and by the initial conditions

$$\theta_s(0,z) = \theta_{s,0}(z)\,, \tag{4a}$$

$$\theta_a(0,z) = \theta_{a,0}(z)\,, \tag{4b}$$

$$x_{a,j}(0,z) = x_{a,j,0}(z)\,, \quad j=1,\ldots,n\,, \tag{4c}$$

$$\theta_c(0,z) = \theta_{c,0}(z)\,, \tag{4d}$$

$$x_{c,j}(0,z) = x_{c,j,0}(z)\,, \quad j=1,\ldots,n\,. \tag{4e}$$

By (3a) and (3b) the thermal insulation of the electrode/electrolyte compound against the surrounding gas is described. Eqs. (3c)–(3e) describe the conditions at the anode inlet. Here the functions $\theta_{a,\mathrm{in}}(\tau)$, $x_{a,j,\mathrm{in}}(\tau)$, $g_{a,\mathrm{in}}(\tau)$ can also serve as input variables. Eqs. (3f)–(3h) describe the conditions at the cathode inlet, which is connected with the anode outlet via the combustion chamber. Here the functions $\theta_{c,\mathrm{in}}$, $x_{c,j,\mathrm{in}}$, $g_{c,\mathrm{in}}$ describe the catalytic combustion of the exhaust anode gas. This combustion process may also be controllable by feeding air from the cell's outside; see again Fig. 1. However, the functions $\theta_{s,0}(z)$, $\theta_{a,0}(z)$, $x_{a,j,0}(z)$, $\theta_{c,0}(z)$, and $x_{c,j,0}(z)$ representing the initial conditions (4) at time $t = 0$ must be prescribed in any case.

For the complete second model (1), (2) additional initial conditions must be prescribed besides (3) and (4):

$$\Phi_a(0,z) = \Phi_{a,0}(z)\,, \tag{5a}$$

$$\Phi_e(0,z) = \Phi_{e,0}(z)\,, \tag{5b}$$

$$\Phi_c(0,z) = \Phi_{c,0}(z)\,, \tag{5c}$$

$$V(0) = V_0\,. \tag{5d}$$

The model is governed by different time constants. While the charge balances (2) are very fast, the energy and mass balances in the gas phases (1b–1g) are slower by several orders of magnitude. The solid temperature is governed by time constants which are even larger than those by three to four orders of magnitude. This can be used to establish further models by assuming steady state for the charge balances together with energy and mass balances in the gas phases. This is done by setting the appropriate time derivatives to zero and allows to simulate medium and long time behaviour.

The model is completely formulated in dimensionless terms and can easily be extended to describe spatially two-dimensional cross-flow systems as well as spatially three-dimensional cell stacks.

3 Index analysis of the PDAE systems

The PDAE system (1) and its augmented version (1), (2) both match the following form

$$A\,u_\tau + B\,u_{zz} + C[u]\,u_z + \psi(\tau,z,u) = 0 \tag{6}$$

with

$$A = \begin{bmatrix} 1 & 0 & 0 \\ 0 & I & 0 \\ 0 & 0 & 0 \end{bmatrix}, \quad B = \begin{bmatrix} -\lambda & 0 & 0 \\ 0 & 0 & 0 \\ 0 & 0 & 0 \end{bmatrix}, \quad C[u] = \begin{bmatrix} 0 & 0 & 0 \\ 0 & C_{22}[u] & 0 \\ 0 & C_{32}[u] & C_{33}[u] \end{bmatrix},$$

when choosing the partition

$$u = (\theta_s \,|\, \theta_a, \theta_c, x_a, x_c \,|\, g_a, g_c)$$

and, resp.,

$$u = (\theta_s \,|\, \theta_a, \theta_c, x_a, x_c, \Phi_a, \Phi_e, \Phi_c, V \,|\, g_a, g_c, i)\,.$$

Here, the matrix $C_{22}[u]$ is nonlinear and the matrices $C_{32}[u]$ and $C_{33}[u]$ are linear. After a coordinate transformation

$$v_a := \theta_a\, g_a\,, \quad v_c := \theta_c\, g_c \tag{7}$$

replacing g_a and g_c, we end up with a linear matrix $C_{22}[u]$, a null matrix C_{32}, and a constant matrix C_{33}.

Hence, the dependent variable u is partioned according to

$$u = (u^{\mathrm{I}}|u^{\mathrm{II}}|u^{\mathrm{III}}) = \begin{cases} (\theta_s|\theta_a, \theta_c, x_a, x_c|v_a, v_c) & \text{for (1) after (7),} \\ (\theta_s|\theta_a, \theta_c, x_a, x_c, \Phi_a, \Phi_e, \Phi_c, V|v_a, v_c, i) & \text{for (1, 2) after (7).} \end{cases} \tag{8}$$

3.1 Time index

In Lucht and Debrabant [5] a special PDAE of type (6) is investigated,

$$A u_\tau + B\, u_{zz} + C[u]\, u_z + D\, u = f(\tau, z)\,, \tag{9}$$

where the matrix $C[u]$ is linear as for (6) after the transformation (7). For this type of PDAE, Lucht and Debrabant define a differential time index as follows: If the matrix A is regular, the time index ν_τ of the PDAE (9) is defined to be zero. If A is singular, then ν_τ is the smallest number of times, the PDAE must be differentiated with respect to τ, in order to determine u_τ as a continuous function of τ, z, u and certain space derivatives of components of u. This definition carries over to eq. (6), too. A similar procedure for a semi-linear first order PDAE is described in [6].

We are now going to compute the time index ν_τ for model (1) after the transformation (7). We start with (1d), (1g), i. e.,

$$0 = \frac{\partial v_a}{\partial z} + \varphi_4(\theta_s, \theta_a, x_a, \Phi_a)\,, \tag{10a}$$

$$0 = \frac{\partial v_c}{\partial z} + \varphi_7(\theta_s, \theta_c, x_c, \Phi_c)\,, \tag{10b}$$

differentiate both equations with respect to τ and substitute the right hand sides of (1) (and (2), if model (1), (2) is investigated):

$$0 = \frac{\partial^2 v_a}{\partial z \partial \tau} + \psi_a(u^{\mathrm{I}}_{zz}, u^{\mathrm{II}}_z, u)\,, \tag{11a}$$

$$0 = \frac{\partial^2 v_c}{\partial z \partial \tau} + \psi_c(u^{\mathrm{I}}_{zz}, u^{\mathrm{II}}_z, u)\,. \tag{11b}$$

These equations can be solved for

$$\frac{\partial v_a}{\partial \tau} = -\int_0^z \psi_a(u^{\mathrm{I}}_{zz}, u^{\mathrm{II}}_z, u)\,\mathrm{d}\bar{z}\,, \tag{12a}$$

$$\frac{\partial v_c}{\partial \tau} = -\int_0^z \psi_c(u^{\mathrm{I}}_{zz}, u^{\mathrm{II}}_z, u)\,\mathrm{d}\bar{z}\,. \tag{12b}$$

The right hand sides of these equations are continuous functions with suitable integrands ψ_a and ψ_c, resp. Therefore the time index is $\nu_\tau = 1$.

For model (1), (2) we additionally have to take into account (2e). Differentiation with respect to τ and substitution of the right hand sides of (2) yield

$$\frac{i - i_a}{c_a} + \frac{i - i_e}{c_e} + \frac{i - i_c}{c_c} + \frac{1}{c_v} \left(\int_0^1 i(\tau, \bar{z}) \, \mathrm{d}\bar{z} - I_{\mathrm{cell}}(\tau) \right) = 0 \,. \tag{13}$$

Since the derivative $\frac{\partial i}{\partial \tau}$ does not appear, we have to differentiate the equation again:

$$\beta \, \frac{\partial i}{\partial \tau}(\tau, z) + \int_0^1 \frac{\partial i}{\partial \tau}(\tau, \bar{z}) \, \mathrm{d}\bar{z} + \psi(u^{\mathrm{I}}_{zz}, u^{\mathrm{II}}_z, u, \frac{\mathrm{d}I_{\mathrm{cell}}}{\mathrm{d}\tau}) = 0 \tag{14}$$

with a suitable function ψ and $\beta := \frac{c_v}{c_a} + \frac{c_v}{c_e} + \frac{c_v}{c_c}$. This is a linear Fredholm integral equation of second kind for the function $w(z) := \frac{\partial i}{\partial \tau}(z, \tau)$. The associated homogeneous integral equation

$$\beta \, w(z) + \int_0^1 w(\bar{z}) \, \mathrm{d}\bar{z} = 0 \tag{15}$$

has the unique solution $w(z) \equiv 0$, since $\beta \neq -1$ for the given data. Therefore eq. (14) is uniquely solvable for

$$\frac{\partial i}{\partial \tau} = \bar{\psi}(u^{\mathrm{I}}_{zz}, u^{\mathrm{II}}_z, u, \frac{\mathrm{d}I_{\mathrm{cell}}}{\mathrm{d}\tau}) \tag{16}$$

with another suitable continuous function $\bar{\psi}$. As a result we obtain that model (1), (2) has time index $\nu_\tau = 2$.

3.2 Spatial index

The definition of the spatial index in [5] can be carried over to the more general eq. (6). Obviously the spatial index of model (1) is $\nu_z = 0$, since all factors in front of the highest spatial derivatives do not vanish.

We are now going to investigate the spatial index for model (1), (2). Since V does not depend on z, it is sufficient, to differentiate eqs. (2a–2c) and (2e) only with respect to z. Choosing suitable continuous functions χ_j, one obtains

$$\begin{bmatrix} \frac{\partial}{\partial \tau} + \frac{1}{c_a} \frac{\partial i_a}{\partial \Phi_a} & 0 & 0 & -\frac{1}{c_a} \\ 0 & \frac{\partial}{\partial \tau} - \frac{1}{c_e} \frac{\partial i_e}{\partial \Phi_e} & 0 & \frac{1}{c_e} \\ 0 & 0 & \frac{\partial}{\partial \tau} - \frac{1}{c_c} \frac{\partial i_c}{\partial \Phi_c} & \frac{1}{c_c} \\ -1 & 1 & 1 & 0 \end{bmatrix} \begin{bmatrix} \frac{\partial \Phi_a}{\partial z} \\ \frac{\partial \Phi_e}{\partial z} \\ \frac{\partial \Phi_c}{\partial z} \\ \frac{\partial i}{\partial z} \end{bmatrix} = \begin{bmatrix} \chi_1(u^{\mathrm{I}}_z, u^{\mathrm{II}}_z) \\ -\chi_2(u^{\mathrm{I}}_z, u^{\mathrm{II}}_z) \\ -\chi_3(u^{\mathrm{I}}_z, u^{\mathrm{II}}_z) \\ 0 \end{bmatrix} = \begin{bmatrix} \tilde{\chi}_1(u, u_t, u^{\mathrm{I}}_z) \\ -\tilde{\chi}_2(u, u_t, u^{\mathrm{I}}_z) \\ -\tilde{\chi}_3(u, u_t, u^{\mathrm{I}}_z) \\ 0 \end{bmatrix} . \tag{17}$$

The derivative $u^{\mathrm{I}}_z = \frac{\partial \theta_s}{\partial z}$ as argument of the functions χ_j is obtained by integrating eq. (1a) with respect to z. We have to show that this operator equation allows a continuous solution. Therefore we investigate a differential algebraic equation system in time of following type:

$$\begin{bmatrix} \frac{\partial}{\partial \tau} + \xi_1(\tau) & 0 & 0 & -\frac{1}{c_a} \\ 0 & \frac{\partial}{\partial \tau} - \xi_2(\tau) & 0 & \frac{1}{c_e} \\ 0 & 0 & \frac{\partial}{\partial \tau} - \xi_3(\tau) & \frac{1}{c_c} \\ -1 & 1 & 1 & 0 \end{bmatrix} \begin{bmatrix} w_1(\tau) \\ w_2(\tau) \\ w_3(\tau) \\ w_4(\tau) \end{bmatrix} = \begin{bmatrix} \bar{\chi}_1(\tau) \\ -\bar{\chi}_2(\tau) \\ -\bar{\chi}_3(\tau) \\ 0 \end{bmatrix} . \tag{18}$$

If we substitute the first three equations into the last equation after differentiating it with respect to τ, we obtain

$$\left(\frac{1}{c_a} + \frac{1}{c_e} + \frac{1}{c_c} \right) w_4 = \sum_{j=1}^{3} \xi_j \, w_j - \sum_{j=1}^{3} \bar{\chi}_j \,. \tag{19}$$

This equation can be solved for w_4 if $\beta \neq 0$ and inserted into the first three equations. This yields a linear inhomogeneous system of ordinary differential equations whose solutions are continuous. In order to have a continuous solution of the operator equation (17), we have to guarantee consistency of the differential algebraic system, i. e., we must not require initial conditions for $w_4(0) = \frac{\partial i}{\partial z}(0, z)$. Then the spatial index for model (1), (2) is $\nu_z = 1$.

4 Index analysis of the MOL system

After an equidistant semi-discretization in space we get a semi-explicit differential algebraic equation system in time τ for the variables $U = (u^1, \ldots, u^M)$, M odd, with $u^j(\tau) \approx u(\tau, z_j)$:

$$\mathcal{A}\frac{d}{d\tau}U + b(U) = 0 \tag{20}$$

with the block diagonal matrix $\mathcal{A} = \mathrm{diag}(\mathcal{A}_1, \ldots, \mathcal{A}_1)$, where $\mathcal{A}_1 = \mathrm{diag}(I, 0)$. The spatial derivatives of u^{II} and u^{III} are approximated by upwind formulas of order 1, the second spatial derivative of θ_s is approximated by the central difference quotient.

We are now going to determine the differentiation index of (20) for model (1) modifying an idea of [1]. The discretized version of (10) reads as follows

$$0 = \frac{v_a^j - v_a^{j-1}}{h} + \varphi_4(\theta_s^j, \theta_a^j, x_a^j, \Phi_a^j)\,, \quad \text{for } j = 2, \ldots, M\,, \tag{21a}$$

$$0 = \frac{v_c^{j+1} - v_c^j}{h} + \varphi_7(\theta_s^j, \theta_c^j, x_c^j, \Phi_c^j)\,, \quad \text{for } j = 1, \ldots, M-1\,. \tag{21b}$$

Here, v_a^1 resp. v_c^M are given by (3c), (3e), resp. (3f), (3h).

Differentiation of eqs. (21a) yields

$$\begin{bmatrix} 1 & & & \\ -1 & 1 & & \\ & \ddots & \ddots & \\ & & -1 & 1 \end{bmatrix} \begin{bmatrix} \frac{\mathrm{d}}{\mathrm{d}\tau} v_a^2 \\ \frac{\mathrm{d}}{\mathrm{d}\tau} v_a^3 \\ \vdots \\ \frac{\mathrm{d}}{\mathrm{d}\tau} v_a^M \end{bmatrix} = -\bar{\varphi}_4(U^{\mathrm{I}}, U^{\mathrm{II}})\,. \tag{22}$$

An analogous result holds for (21b). Obviously, the coefficient matrix is regular. Therefore the differential index of the system (20) is $\nu_{\mathrm{MOL}} = 1$, which coincides in this case with the perturbation index of the system (20).

Next we determine the differentiation index of (20) for model (1), (2). We first substitute the integral $\int_0^1 i(\tau, \bar{z})\,\mathrm{d}\bar{z}$ in eq. (2d) by a quadrature formula of type $\sum_{k=1}^M \omega_k\, i(\tau, z_k)$ with $\sum_{k=1}^M \omega_k = 1$ and $\omega_k > 0$, e. g., Simpson's rule. Differentiating the semi-discretized eq. (2e) and substituting the semi-discretized eqs. (2a)–(2d) yields

$$\frac{i - i_a|_{(\tau,z_l)}}{c_a} + \frac{i - i_e|_{(\tau,z_l)}}{c_e} + \frac{i - i_c|_{(\tau,z_l)}}{c_c} + \frac{1}{c_v}\left(\sum_{k=1}^M \omega_k\, i(\tau, z_k) - I_{\mathrm{cell}}(\tau)\right) = 0 \tag{23}$$

respectively,

$$\mathcal{G}\begin{bmatrix} i(\tau, z_1) \\ \vdots \\ i(\tau, z_M) \end{bmatrix} = \gamma(U^{\mathrm{I}}, U^{\mathrm{II}}, I_{\mathrm{cell}})\,. \tag{24}$$

Here, $\mathcal{G} = \mathrm{diag}(\beta, \ldots, \beta) + (1, \ldots, 1)^\top(\omega_1, \ldots, \omega_M)$, and U^{I}, U^{II} are the discretized values of u^{I} and u^{II}, resp. The matrix $\mathcal{G}$ is obviously diagonal-dominant for $\beta > 1$, since $\sum_{k=1}^M \omega_k = 1$ and $\omega_k > 0$.

After another differentiation step we can solve for $\frac{\partial i}{\partial \tau}(\tau, z_j)$, $j = 1, \ldots, M$. Hence, the semi-discretized model (1), (2) has differentiation index $\nu_{\mathrm{MOL}} = 2$.

5 Numerical results

The numerical procedure for the solution of system (1), (2) is the vertical method of lines based on the discretization described in Sect. 4. For the simulation the software package EASY-FIT (see [10] and [11]) is used, which is appropriate for parameter identification and optimization of those systems, too. The resulting DAE system (20) is thereby integrated using a RADAU 5-method.

The following figures show the numerical results obtained [7, 9]. While most of the variables seem to have reached a stationary state at the final time τ_f of the simulation, the solid temperature θ_s does not. This is due to the fact, that different

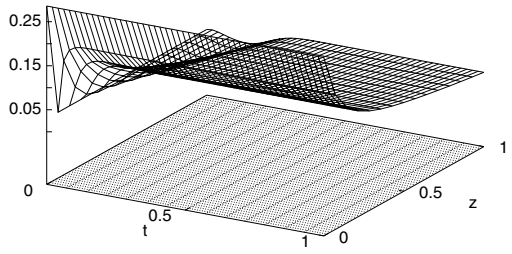

Fig. 2 Molar fraction of methane $\mathrm{CH_4}$ in the anode channel.

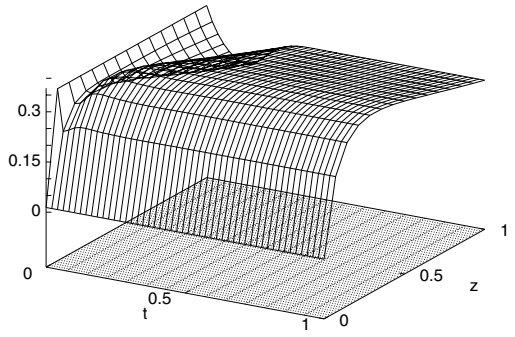

Fig. 3 Molar fraction of hydrogen $\mathrm{H_2}$ in the anode channel.

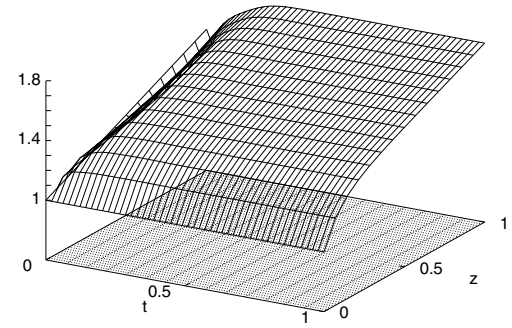

Fig. 4 Molar flow g_a in the anode channel.

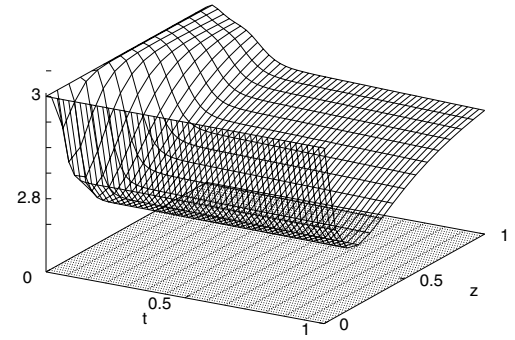

Fig. 5 Temperature θ_a of the anode gas.

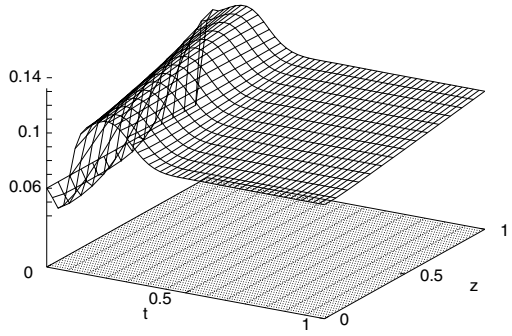

Fig. 6 Molar fraction of oxygen $\mathrm{O_2}$ in the cathode channel.

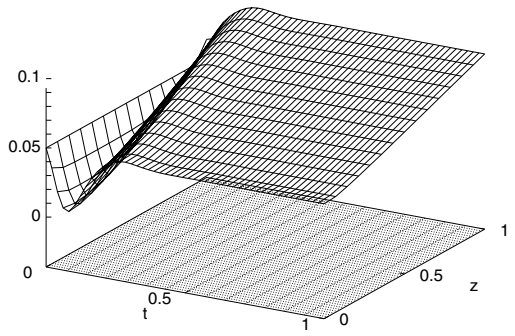

Fig. 7 Molar fraction of carbon dioxide $\mathrm{CO_2}$ in the cathode channel.

time constants are present. The solid temperature is here the slowest variable because of the large heat capacity of the cell stack. Thus the Figs. 2–9 show a quasistationary behaviour so far.

Fig. 2 shows the dynamic behaviour of the molar fraction for methane in the anode channel over the space time grid. Methane enters the anode channel with a high concentration. Then it is used for the internal reforming reaction until a reaction equilibrium is nearly obtained in space direction. Simultaneously the molar fraction of hydrogen in the anode channel (Fig. 3) increases firstly in space direction, since it is produced by the internal reforming, whereas it later on decreases, since it is consumed in the oxidization reaction at the anode electrode. Because of the increasing number of molecules in the gas stream the molar flow g_a in the anode channel (Fig. 4) also increases over the space variable. Since the endothermic reforming reaction takes place near the anode inlet ($z = 0$), the anode gas temperature θ_a is decreased along the spatial coordinate z. The exothermic electochemical reactions occur along the whole channel and heat up the solid cell parts. From these, the anode gas is heated up again; see Fig. 5.

The situation in the cathode channel is mainly described by the molar fractions of oxygen (Fig. 6) and carbon dioxide (Fig. 7). Since these substances are used in the cathode reaction, the associated molar fractions decrease from the cathode inlet ($z = 1$) to the outlet ($z = 0$) monotonously.

Fig. 8 shows the current density distribution. It seems to be dominated by the concentrations of the electrochemical reaction educts in the cathode channel, oxygen and carbon dioxide.

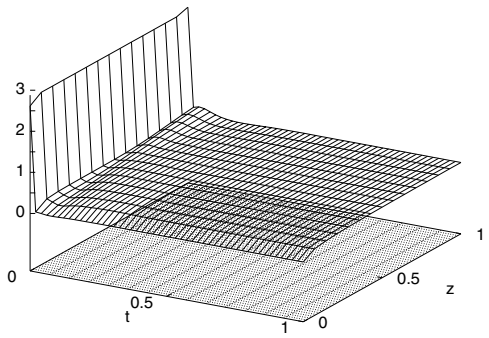

Fig. 8 Current density i.

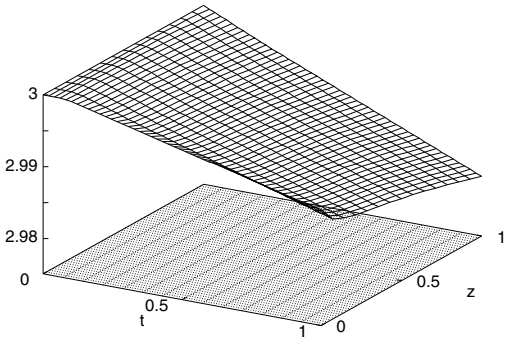

Fig. 9 Solid temperatur θ_s.

Finally Fig. 9 shows the behaviour of the solid temperature θ_s. It decreases slowly, since the sum of the heat, which is detracted by convection through the cathode gas stream and by the inflow of cold air through the catalytic burner into the fuel cell, is greater than the heat generated by the chemical reactions. Thus the fuel cell stack cools down in the present simulation.

6 Conclusion and outlook

The model presented in this paper describes the dynamical behaviour of a molten carbonate fuel cell stack. It is not only interesting from an engineering point of view because MCFC stacks provide an environmentally friendly energy production, but also from the point of view of applied mathematics: The model generalizes certain types of partial differential algebraic equations currently under research and yields a challenging optimization problem with (singular) PDE constraints. In the present paper, a detailed index analysis is performed. As subproblems of the index analysis appear integral equations and differential-algebraic equations in one variable. The index analysis is the basis for first numerical simulations. These first simulations and their associated numerical results are presented here for a spatially one-dimensional PDAE model. Further investigations will be concerned with both more detailed and simplified models, in order to establish a hierarchy of embedded models. They will differ in spatial dimension, in their way to approximate the steady state at different time scales and in their associated indices following the lines of this paper. At the end, an optimization shall be performed to control fuel cell stacks in start-up and shut-down situations and in case of load changes. The hierarchically ordered models will be used for model reduction in the optimization process in order to reduce the excessively high computing times.

Acknowledgements This work is supported by the German Federal Ministry of Education and Research (BMBF) within the project Optimierte Prozessführung von Brennstoffzellensystemen mit Methoden der Nichtlinearen Dynamik.

References

[1] M. Günther and Y. Wagner, SIAM J. Sci. Comput. **22**, 1610–1629 (2000).
[2] P. Heidebrecht and K. Sundmacher, Chem. Eng. Sci. **58**, 1029–1036 (2003).
[3] P. Heidebrecht and K. Sundmacher, Fuel Cells **3–4**, 166–180 (2002).
[4] G. Huppmann, Das MTU Direkt-Brennstoffzellen Hot Module (MCFC), in: Brennstoffzellen – Entwicklung, Technologie, Anwendung, edited by K. Ledjeff-Hey et al. (C. F. Müller, Heidelberg, 2001).
[5] W. Lucht and K. Debrabant, Appl. Numer. Math. **42**, 297–314 (2002).
[6] W. S. Martinson and P. I. Barton, SIAM J. Sci. Comput. **21**, 2295–2315 (2000).
[7] V. Petzet, Numerische Simulation von Schmelzkarbonat-Brennstoffzellen: 1-D-PDAE-Modelle, ihr Differentiationsindex und ihre numerische Diskretisierung, Diploma Thesis, Chair of Mathematics in Engineering Sciences, University of Bayreuth, Bayreuth, Germany (2003).
[8] S. Rolf, Betriebserfahrungen mit dem MTU Hot Module, in: Stationäre Brennstoffzellenanlagen. VDI Berichte Nr. 1596, VDI Verlag, Düsseldorf, Germany, 2001.
[9] S. Scherdel, Numerische Simulation von Schmelzkarbonat-Brennstoffzellen: 1-D-PDAE-Modelle, ihr MOL-Index und ihre numerische Diskretisierung, Diploma Thesis, Chair of Mathematics in Engineering Sciences, University of Bayreuth, Bayreuth, Germany (2003).
[10] K. Schittkowski, Struct. Multidiscip. Optim. **23**(2), 153–169 (2002).
[11] K. Schittkowski, Numerical Data Fitting in Dynamical Systems (Kluwer, Boston, 2002).
[12] K. Sundmacher and U. Hoffmann, J. Appl. Electrochem. **28**, 359–368 (1998).
[13] W. Winkler, Brennstoffzellenanlagen (Springer, Berlin, 2002).